

---

# Morphological Synthesis and workspace design for a parallel manipulator with linear actuators

Carlos Andrés Mesa-Montoya, Héctor Fabio Quintero-Riaza & Federico Gutiérrez-Madrid

Facultad de Ingeniería Mecánica, Universidad Tecnológica de Pereira, Pereira, Colombia. [caanmesa@utp.edu.co](mailto:caanmesa@utp.edu.co), [hquinte@utp.edu.co](mailto:hquinte@utp.edu.co), [fede9506@utp.edu.co](mailto:fede9506@utp.edu.co)

Received: July 4<sup>th</sup>, 2019. Received in revised form: March 17<sup>th</sup>, 2020. Accepted: March 30<sup>th</sup>, 2020.

## Abstract

This paper addresses the kinematic structure and workspace analysis of a parallel manipulator with linear actuators considering two studies. The first one was based on a morphological synthesis in which a kinematic connections approach was implemented. The set of combinations of joints and links for the desired system and their linkage are illustrated. Finally, the development regarding the conceivable morphology is detailed, providing three linear degrees of freedom between the mobile and fixed platforms. The second study presented the dimensional synthesis of the manipulator, considering a workspace required and an input transmission index. The geometrical design was based on the maximum inscribed workspace volume; the cylindrical shape radius inscribed on a workspace intersection is also exemplified. The geometric determination of the workspace for the manipulator was demonstrated using computer-aided design. A design result of the Delta as checked with the stiffness and condition indices.

**Keywords:** dimensional synthesis; kinematics design; morphological synthesis; parallel manipulator; workspace.

---

# Síntesis morfológica y dimensional de un manipulador paralelo con actuadores lineales

## Resumen

Este artículo aborda el análisis cinemático y el espacio de trabajo de un manipulador paralelo con actuadores lineales considerando dos estudios. El primero trata sobre la síntesis morfológica, implementando un acercamiento por medio del método de juntas cinemáticas. Son ilustrados el conjunto de combinaciones de las juntas y pares para el sistema deseado y sus relaciones. Finalmente, se detalla el desarrollo de la morfología concebida, la cual provee tres grados de libertad lineales entre la plataforma fija y móvil. El segundo estudio presenta la síntesis dimensional del manipulador, considerando un espacio de trabajo requerido y un índice de transmisión de entrada. El diseño geométrico utiliza el máximo volumen de trabajo inscrito; se muestra la geometría cilíndrica inscrita en la intersección con espacio de trabajo. Se determina la geometría del espacio de trabajo utilizando CAD y el diseño resultante del Delta es verificado con el índice de rigidez y de condición.

**Palabras clave:** diseño cinemático; espacio de trabajo; manipulador paralelo; síntesis dimensional; síntesis morfológica.

---

## 1. Introduction

A large variety of architectures exist in the family of robots, the most popular ones in the industry being parallel and serial manipulators. In serial manipulators, the actuators are located along their mechanical structure, generating an increase in the inertia that the robot must overcome to move; this means that the more actuators the robot has, the higher

the charge on it is, affecting the stability of the entire mechanism. Additionally, each actuator increases the probability of generating an error of position and orientation of the terminal tool coupled to the mobile platform [1].

For this reason, parallel manipulators emerged, in which two or more kinematic chains support the mobile platform, increasing its stiffness, stability, load capacity and precision of position, orientation, velocity and acceleration of the final

---

**How to cite:** Mesa-Montoya, C.A., Quintero-Riaza, H.F., and Gutiérrez-Madrid, F. Morphological Synthesis and Workspace Design for a Parallel Manipulator with Linear Actuators. DYNA, 87(213), pp. 129-139, April - June, 2020.

actuator, and the entire robot [2]. These advantages make these robots adequate for applications such as a) machining processes, b) mounting, c) manipulation, d) transport and e) storage [3].

Because of the importance of these robots, this paper addresses the kinematic, structural, and workspace analysis of a manipulator with linear actuators with consideration to two studies.

The first study examined the morphological synthesis of diverse solutions for kinematic chain structures for parallel manipulators of low mobility. This has been the focus of much research over the last few decades, resulting in four frequently used methods for morphological synthesis today: a) the screw theory [7], b) theory of displacement groups [8-10], c) theory of lineal transformations [11-13], and d) kinematic connections [1,14]. In this paper, the method of kinematic connections is used through the methodology proposed by Zhang [1]. Subsequently, the Chebychev-Grübler-Kutzbach criterion is introduced. The set of combinations of joints and links for the desired system and their linkage, omitting geometric details such as the link length and distribution, are illustrated. Finally, the development regarding the conceivable morphology is detailed, providing three linear degrees of freedom between the mobile and fixed platforms.

The second study examined the dimensional synthesis of the selected manipulator. To satisfy the demands for the design of these manipulators, the academic community has conducted various research that aims to establish methods involving numeric techniques of optimization [21,22], performance maps [23,24], and a maximum inscribed workspace [17], to guarantee a workspace that is as regular as possible. For the development of this study, the method of maximum inscribed workspace proposed by Lui [17] was used, incorporating an input transmission index [16]. Additionally, the cylindrical shape radius inscribed on the workspace intersection was exemplified. The geometric determination of the workspace for the manipulator was demonstrated using computer-aided design (CAD).

## 2. Methods

### 2.1. Preliminary restrictions of the manipulator

The border conditions or dimensional restrictions of the manipulator are the results of the settling of the workspace conditions, where the manipulator demonstrates its greater ability, and which have a low possibility of manifesting singular positions on its mobile elements. Table 1 shows the maximum permissible restrictions for the components of the manipulator, and the workspace dimensions according to the technical specifications of parallel manipulators of similar architecture that are used for commercial purposes [4,5].

### 2.2. Morphological synthesis

Table 2 shows the synthesis method of kinematic connections proposed by Zhang [1] for full isotropic parallel manipulators.

Table 1.  
Structural requirements.

Characteristics	Preliminary Restrictions	Restrictions
Structural	Fixed platform radius	310-500 mm
	Leg length	150-300 mm
	Forearm length	290-500 mm
	Mobile platform radius	50-300 mm
Workspace	Maximum cross-sectional dimension (cylindrical shape)	150-265 mm
	Maximum cross-sectional dimension (cuboid)	106-187 mm
	Maximum Z Height	235-400 mm

Source: The Authors.

Table 2.  
Synthesis methodology of full-isotropic parallel manipulators.

Stage	Objectives	Activities
1	Establishing possible structures	Alternatives for the kinematic chain. Structure of the vertexes of connection. Structures for the mobile and fixed platforms.
	Construction of architectures	To scheme possible architectures for the manipulator. To consider the number and type of degrees of freedom in the kinematic joints.
	Selection of the most promising architecture	To look for practicality and simplicity. To eliminate kinematic joints of the prismatic type that may generate passive conditions. To eliminate the rotation along the perpendicular axis to the plane of the fixed platform. To look for symmetric structures.

Source: The Authors.

#### 2.2.1. Design criteria

The structural conditions considered in the synthesis process are the following: a) manipulator with three degrees of freedom, b) fully-isotropic parallel manipulator, c) two known elements (fixed and mobile platform), and d) three parallel kinematic chains.

To determine the possible degrees of freedom provided by each kinematic chain in the manipulator, we evaluated the mobility of the kinematic chain using the Chebychev-Grübler-Kutzbach formula [15], along with the contribution of Tsai [15] to the passive degrees of freedom:

$$M = d(n - g - 1) + \sum_{i=1}^g f_i - f_g \quad (1)$$

where  $M$  is the degrees of freedom of the kinematic chain;  $d$  is the degrees of freedom of the individual elements without restricting (6 in the spatial scenario and 3 in the plane scenario);  $n$  is the number of rigid bodies, elements, or links of the kinematic chain;  $g$  is the number of joints;  $f_i$  is the

number of degrees of freedom per kinematic pair; and  $f_g$  is the number of passive degrees of freedom in the kinematic chain, and it may take positive values when degrees of freedom are available (not transferred to the terminal element) or negative values when there are additional restrictions to the movement.

### 2.2.2. Distribution of degrees of freedom per kinematic chain.

The different configurations of elements and joints that consolidate the kinematic chain can be determined by considering the different assumptions established to each of the parameters of Eq. (1). First, the equations that enable determining the number of elements in the kinematic chain, in function of the joints are defined:

$$n = 2 + n_{cc} \quad (2)$$

$$n_{cc} \begin{cases} \sum_{j=1}^L (f_{lj} - 1) & \text{Binary} \\ \sum_{j=1}^L (f_{lj} - 2) & \text{Ternary} \end{cases} \quad (3)$$

where  $n$  is the number of elements that consolidate the parallel manipulator, 2 represents the two platforms (fixed and mobile), and  $n_{cc}$  is the set of elements that consolidate the parallel kinematic chains, which can be calculated in two different ways:

- a) Considering each element as binary regarding the number of joints,
- b) Considering that at least one element per kinematic chain is ternary.

The total number of joints in the manipulator can be expressed as follows:

$$g = \sum_{j=1}^L f_j \quad (4)$$

Substituting Eqs. (2)-(4) into (1) results in  $M$  for the scenario of binary elements (5) and ternaries (6):

$$M = 6[1 - L] + \sum_{j=1}^g f_{lj} - f_g \quad (5)$$

$$M = 6[1 - 2L] + \sum_{j=1}^g f_{lj} - f_g \quad (6)$$

By knowing the values of  $M$ ,  $L$ , and  $f_g$ , the total degrees of freedom provided by the joints in the kinematic chains that consolidate the manipulator can be determined.

### 2.3. Dimensional synthesis

The purpose of the dimensional synthesis is to determine the primary dimensions (or additional parameters) and initial position of a preconceive mechanism, according to the tasks that are developed. The term "primary dimensions" refers to the lengths of the links, whether they are binary or ternary. The defined dimensional parameters must generate a maximum workspace that accomplishes the following requirements [16]: a) regular form of the workspace according to the application, b) adequate required skill, c) compact configuration, and d) low-cost. Considering the criterion previously defined, the method of maximum inscribed workspace is used [17], incorporating an input transmission index [16].

#### 2.3.1. Input transmission index

The function of the manipulator is to transmit the movement and force of an input link towards an exit link, guaranteeing the transmitted force along the kinematic chains, until the stated element can generate the dynamic equilibrium. Considering that the architecture of the manipulator is completely parallel and only considers one actuator per kinematic chain (considering active prismatic joints, but not the gravitational effects and the friction in the joints), the input transmission index is defined by [16]:

$$\lambda_i = |f_i \cdot v_i| = |\cos\psi| = |\sin\gamma| \quad (7)$$

where  $\lambda_i$  is the input transmission index,  $\gamma$  is the angle of transmission,  $\psi$  is the angle of deviation,  $f_i$  is the static force, and  $v_i$  is the absolute velocity vector.

Fig. 1 shows the inverse transmission and deviation angles, as well as the static force of the coupler:

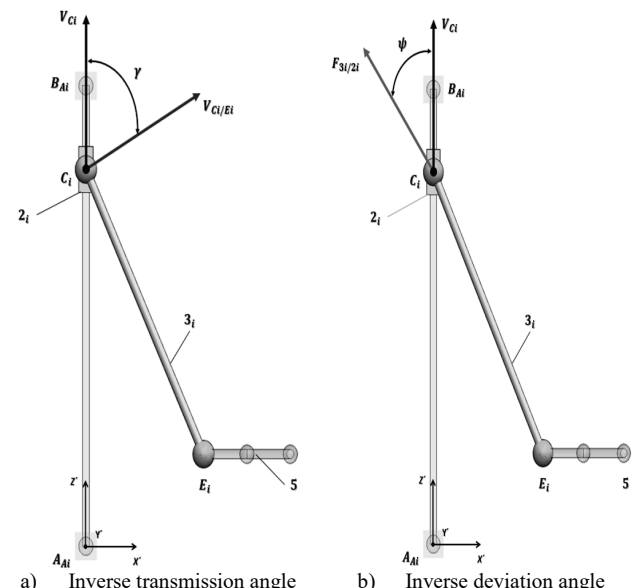


Figure 1. Inverse transmission and deviation angles

Source: The Authors.

The angles  $\gamma$  and  $\psi$ , in Fig. 1 correspond to two criteria of the manipulator's input manipulability. The first angle is known as the transmission angle,  $\gamma$ , and is defined as the lower angle between the relative velocity vector,  $v_{C/E}$ , of the coupler element, and the absolute velocity vector,  $v_C$ , of the input link, both obtained from the kinematic pair, C (Fig. 1 (a)). The other criterion consists of using the direction of the static force transmitted,  $F_{3/2}$ , from the coupler to the input element and the velocity of the connection point,  $v_C$ ; the angle between them is known as deviation angle,  $\psi$ . In the analysed manipulator, the transmission and deviations angles are complementary (Fig. 1 (b)).

According to Tao [18], for systems in which the transmission of movement must be precise and at a high speed, the permissible values for the angle of transmission must be between 45 and 135°. Sharma [19] postulated that an angle of transmission lower than 20° is unacceptable for a mechanism of high velocity. Martin [20] asserted that mechanisms of general purpose must comply with a minimum angle of transmission higher than 40°. For the configuration studied in this project, the angle of transmission could not attain higher values than 90°; otherwise, the mobile platform would have surpassed the plane where the prismatic joints were located, which was not structurally possible to achieve. Taking as reference the previously mentioned, the input transmission index must not be lower than  $\sin 45^\circ \approx 0.7$ . According to Liu [16] when the input transmission index is higher or equal to 0.7, the manipulator possesses an adequate relation of mobility or force. If within the maximum inscribed workspace, the positions of the kinematic chains of the manipulator are guaranteed, values lower to 0.7 will not be presented in the input transmission index, the mobile platform of the manipulator will have an adequate capacity to transmit movement and force, with a low possibility, and singular positions may result [16].

### 2.3.2. Design criteria

To determine the parameters, the method considers a cylindrical workspace of radius  $r_0$  and height  $h$ . From the cylindrical form obtained, an inscribed hexahedron of a similar form can also be defined. In Fig. 2 the mobile platform is considered to move over the horizontal plane with  $z=z_0$  measured in regard to the framework of reference (OXYZ).

$P'$  represents the closer position of the center of the mobile platform with respect to the action line of the prismatic pair  $Q$ , while  $P''$  is the farther position.  $P'H'Q'$  and  $P''H''Q''$  correspond to the kinematic chain orientations when the center of the mobile platform coincides with the borders of the cylinder. In Fig. 3, the orientations that can test the kinematic chain are illustrated according to the extreme positions the mobile platform may reach.

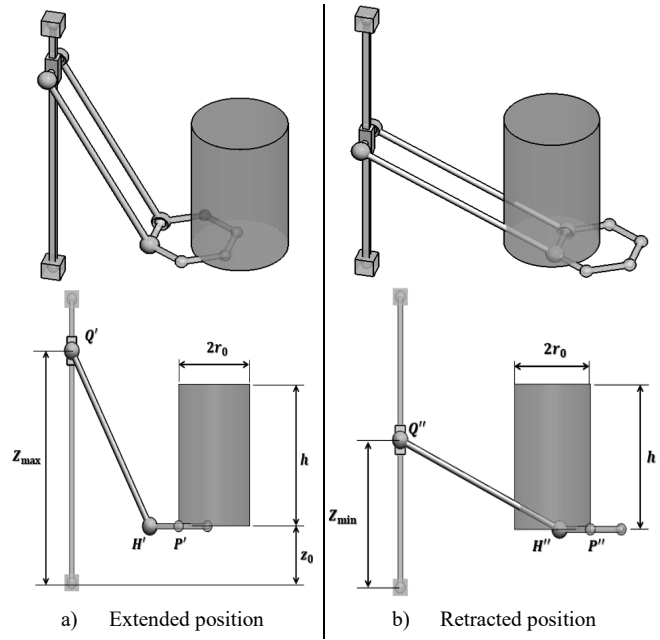


Figure 2. Extreme position of the mobile platform.  
Source: The Authors.

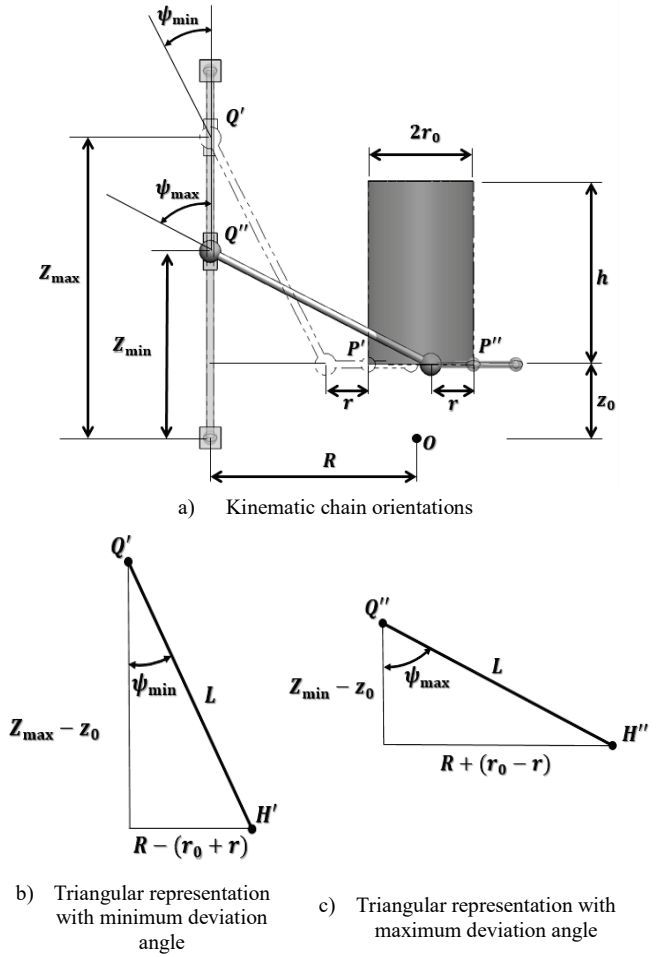


Figure 3. Kinematic chain orientations.  
Source: The Authors.

From Figs. 3 (b) and (c) the following relations are obtained between the dimensional parameters of the manipulator:

$$\sin \psi_{\max} = \frac{R + (r_0 - r)}{L} \quad (8)$$

$$\sin \psi_{\min} = \frac{R - (r_0 + r)}{L} \quad (9)$$

With the aim of establishing a technical condition and structural reliability between the maximum and minimum deviation angles, these are related to the maximum opening angle (in practical terms, the spherical joints have a permissible interval of values for the opening angle between 15 and 30°) that enables the spherical joint  $C_i$ , of the form

$$\rho = \psi_{\max} - \psi_{\min} \quad (10)$$

If the deviation angles are specified, the dimensional parameters  $L$  and  $R-r$  can be determined, using Eq. (9) and (10), in the form

$$L = \frac{2r_0}{\sin \psi_{\max} - \sin \psi_{\min}} \quad (11)$$

$$R - r = L \cdot \sin \psi_{\min} + r_0 \quad (12)$$

Under the same considerations, in Figs. 3 (b) and (c), the range of movement can be determined in the prismatic joints, and it corresponds to the defined height for the manipulator's workspace through the equations.

$$z_{\min} - z_0 = L \cdot \cos \psi_{\max} \quad (13)$$

$$z_{\max} - z_0 = L \cdot \cos \psi_{\min} + h \quad (14)$$

#### 2.4. Jacobian analysis of the manipulator

The Jacobian matrix of a parallel manipulator relates the velocity of the moving platform  $(\dot{u}, \dot{v}, \dot{w})$  and velocity present in the active kinematic pairs  $(\dot{q}_A, \dot{q}_B, \dot{q}_C)$  [1]. The analysis of the Jacobian matrix is used to determine the manipulator's stiffness matrix, which represents the resistance of the manipulator to the external forces applied to the mobile platform, assuming that the elements or links are rigid. Similarly, it represents the mechanical advantage of the manipulator associated with the capacity to transfer the forces from the linear actuators to the mobile platform [25]. Furthermore, the condition number (which is a measure of the sensitivity of the solution of a reversible matrix to the changes that its components can undergo) of the Jacobian matrix can be used to determine the manipulator's dexterity, which is an important kinematic factor that affects the accuracy of the speed and the dead load of the mobile platform [25,32].

$$\begin{aligned} \dot{x} \cdot (x - x_{Si}) + \dot{y} \cdot (y - y_{Si}) + \dot{z} \cdot (z - z_{Si}) - \dot{z}_{Si} \\ \cdot (z - z_{Si}) = 0 \end{aligned} \quad (15)$$

If  $(z_{SA}, z_{SB}, z_{SC}) = (q_A, q_B, q_C)$  and  $(x, y, z) = (u, v, w)$ , then

$$\begin{aligned} \dot{u} \cdot (u - x_{Si}) + \dot{v} \cdot (v - y_{Si}) + \dot{w} \cdot (w - q_i) - \dot{q}_i \\ \cdot (w - q_i) = 0 \end{aligned} \quad (16)$$

Expanding Eqs. (15) and (16) for the three vector loops, we obtain

$$\begin{aligned} & \begin{bmatrix} u - x_{SA} & v - y_{SA} & w - q_A \\ u - x_{SB} & v - y_{SB} & w - q_B \\ u - x_{SC} & v - y_{SC} & w - q_C \end{bmatrix} \begin{Bmatrix} \dot{u} \\ \dot{v} \\ \dot{w} \end{Bmatrix} \\ &= \begin{bmatrix} w - q_A & 0 & 0 \\ 0 & w - q_B & 0 \\ 0 & 0 & w - q_C \end{bmatrix} \begin{Bmatrix} \dot{q}_A \\ \dot{q}_B \\ \dot{q}_C \end{Bmatrix} \end{aligned} \quad (17)$$

In which

$$[J_q] = \begin{bmatrix} w - q_A & 0 & 0 \\ 0 & w - q_B & 0 \\ 0 & 0 & w - q_C \end{bmatrix} \quad (18)$$

$$[J_x] = \begin{bmatrix} u - x_{SA} & v - y_{SA} & w - q_A \\ u - x_{SB} & v - y_{SB} & w - q_B \\ u - x_{SC} & v - y_{SC} & w - q_C \end{bmatrix} = \begin{bmatrix} (P - S_{SA}) \\ (P - S_{SB}) \\ (P - S_{SC}) \end{bmatrix} \quad (19)$$

The Jacobian matrix can be expressed as

$$J = \begin{bmatrix} \frac{(u - x_{SA})}{w - q_A} & \frac{(v - y_{SA})}{w - q_A} & 1 \\ \frac{(u - x_{SB})}{w - q_B} & \frac{(v - y_{SB})}{w - q_B} & 1 \\ \frac{(u - x_{SC})}{w - q_C} & \frac{(v - y_{SC})}{w - q_C} & 1 \end{bmatrix} \quad (20)$$

In which

$$(x_{SA}, y_{SA}) = (0, L_{Rr}) \quad (x_{SB}, y_{SB}) = \left( \frac{\sqrt{3}}{2} L_{Rr}, -\frac{1}{2} L_{Rr} \right)$$

$$(x_{SC}, y_{SC}) = \left( -\frac{\sqrt{3}}{2} L_{Rr}, -\frac{1}{2} L_{Rr} \right)$$

##### 2.4.1. Manipulator's stiffness matrix

Let  $\tau = [\tau_1, \tau_2, \tau_3, \dots, \tau_n]^T$  be the vector of motor forces or torques that act on the manipulator and  $\Delta q =$

$[\Delta q_1, \Delta q_2, \Delta q_3, \dots, \Delta q_n]^T$  the vector of joint displacements. According to Tsai [15], the vectors  $\tau$  and  $\Delta q$  can be related by the equation

$$\tau = \chi \Delta q \quad (21)$$

In which  $\chi = \text{diag}[k_1, k_2, k_3, \dots, k_n]$  is a diagonal  $n \times n$  matrix of the stiffness coefficients for each of the kinematic chains.

The resultant force of the mobile platform is related to the vector of motor forces or torques that act on the manipulator following the equation

$$F = J^t \tau \quad (22)$$

In which  $J^t$ , is the transposed Jacobian matrix.

Joint displacements are related to linear and angular displacements ( $\Delta x = [\Delta x, \Delta y, \Delta z, \Delta \phi, \Delta \theta, \Delta \psi]^T$ ) of the mobile platform following the Jacobian Matrix [15], as:

$$\Delta q = J \Delta x \quad (23)$$

Substituting Eqs. (21) and (23) into (22) we obtain

$$F = K \Delta x \quad (24)$$

In which  $K = J^t \chi J$ , is the manipulator's stiffness matrix.

For the manipulator studied, the three kinematic chains were considered symmetrical and completely rigid; hence, we assumed that the only source of flexibility was concentrated in the active kinematic pair governed by the actuator [15]. Here, the stiffness coefficients were considered equal ( $k_a = k_b = k_c = k_{\text{act}}$ ); thus, the stiffness matrix can be rewritten as follows:

$$K = J^T (k_{\text{act}} \cdot I) J = k_{\text{act}} \cdot J^T J \quad (25)$$

Using Eq. (25) in conjunction with Eq. (20), the stiffness matrix is obtained:

$$K = k_{\text{Act}} \begin{bmatrix} K_{11} & K_{12} & K_{13} \\ K_{21} & K_{22} & K_{23} \\ K_{31} & K_{32} & K_{33} \end{bmatrix} \quad (26)$$

Because Eq. (25) depends on the Jacobian matrix, the stiffness also depends on the position in which the manipulator is; hence, the results obtained are instantaneous. The instantaneous stiffness associated with the mobile platform for each axis is associated with the components of the main diagonal of the stiffness matrix, as shown below:

$$K_{\text{Stx}} = K_{11}$$

$$= k_{\text{Act}} \cdot \left[ \left( \frac{\Delta U_{\text{Sa}}}{\Delta W_{\text{Sa}}} \right)^2 + \left( \frac{\Delta U_{\text{Sb}}}{\Delta W_{\text{Sb}}} \right)^2 + \left( \frac{\Delta U_{\text{Sc}}}{\Delta W_{\text{Sc}}} \right)^2 \right] \quad (27)$$

$$K_{\text{Sty}} = K_{22}$$

$$= k_{\text{Act}} \cdot \left[ \left( \frac{\Delta V_{\text{Sa}}}{\Delta W_{\text{Sa}}} \right)^2 + \left( \frac{\Delta V_{\text{Sb}}}{\Delta W_{\text{Sb}}} \right)^2 + \left( \frac{\Delta V_{\text{Sc}}}{\Delta W_{\text{Sc}}} \right)^2 \right] \quad (28)$$

$$K_{\text{Stz}} = K_{33} = 3 \cdot k_{\text{Act}} \quad (29)$$

In which

$K_{\text{Stx}}$  Instantaneous stiffness of the mobile platform in the x-direction.

$K_{\text{Sty}}$  Instantaneous stiffness of the mobile platform in the y-direction.

$K_{\text{Stz}}$  Instantaneous stiffness of the mobile platform in the z-direction.

The previous results indicate that the stiffness along the z-axis depends only on the stiffness coefficient of the active kinematic pairs governed by the actuator for a given workspace.

The total stiffness ( $K_{\text{STT}}$ ) is determined as the trace of the stiffness matrix:

$$K_{\text{STT}} = \text{tr}(K) = K_{\text{STX}} + K_{\text{STY}} + K_{\text{STZ}} \quad (30)$$

$$= k_{\text{ACT}} \cdot \left\{ 2 \left[ \left( \frac{\Delta U_{\text{SA}}}{\Delta W_{\text{SA}}} \right)^2 + \left( \frac{\Delta U_{\text{SB}}}{\Delta W_{\text{SB}}} \right)^2 + \left( \frac{\Delta U_{\text{SC}}}{\Delta W_{\text{SC}}} \right)^2 \right] + 3 \right\}$$

The stiffness of the active prismatic kinematic pair depends on many factors such as the mechanical components, power of the electric motors, and control system. The authors in [29,30] only considered the effect of the Jacobian Matrix in the stiffness analysis, which is why they assumed  $k_{\text{act}} = 1 \text{ kN/m}$ . For most developed stiffness analyzes, Zhang [1] used a value of  $k_{\text{act}} = 1 \text{ GN/m}$ , whereas Pashkevich [31] proposed a value for linear actuators as  $k_{\text{act}} = 100 \text{ MN/m}$ . For the stiffness analysis developed in this study, the stiffness value for the linear actuators was considered as  $k_{\text{act}} = 100 \text{ MN/m}$ , which represented an intermediate value for initial design purposes.

#### 2.4.2. Condition index

The dexterity analysis is directly related to the condition index (CI) which is the reciprocal of the conditioning number Eq. (31) of the Jacobian matrix [16,33].

$$CI = \frac{1}{\kappa} \quad (31)$$

where  $\kappa$  is the condition number, which is determined by the multiplication of any of the rules of the Jacobian matrix and its inverse, that is

$$\kappa = \|J^{-1}\| \|J\| \quad (32)$$

Another approach to calculating the condition number is in terms of the stiffness matrix and its eigenvalues:

$$\kappa = \sqrt{\frac{\lambda_1}{\lambda_2}} \quad (33)$$

In which

$\lambda_1$  Maximum eigenvalue of the stiffness matrix  $K$ .

$\lambda_2$  Minimum eigenvalue of the stiffness matrix  $K$ .

The condition index can have a value between 0 and 1, which enables the skill, manipulator's isotropy level (the ability to transmit movement and static charge in all directions), and the remoteness of the manipulator of singular positions to be determined [33]. When  $CI = 0$ , the robot is in a singular position, at which it is considered to be in a state out of control [17]. When  $CI = 1$ , the manipulator is in an isotropic configuration.

### 3. Results

#### 3.1. Viable morphologic structures

Table 3 shows the different alternatives or compound structural configurations for binary and ternary elements, achieving the defined requisites in Eqs. (5) and (6).

#### 3.2. Morphological structure selected

The result obtained when the proposed methodology by Zhang [21] was implemented for the morphological synthesis process was that the structure of the manipulator that fulfilled the established design criteria was a  $3\underline{P}Pa^{4S}$  type, which required the use of the structure of the mobile platform with binary vertexes (Fig. 4). The spatial kinematic scheme of the manipulator is shown in Fig. 5.

Table 3.  
Synthesis methodology of full-isotropic parallel manipulators.

Alternatives	Element types	Structural configurations
1		1P1R1S
2		1P2R1H
3		1P1P1R1H
4		1P2P1H
5	Binary	1P4R
6		1P1P3R
7		1P2P2R
8		1P3P1R
9		1P4P
10	Binaries and ternaries	1PRPaR
11	ternaries	1PPa <sup>4S</sup>

Source: The Authors.

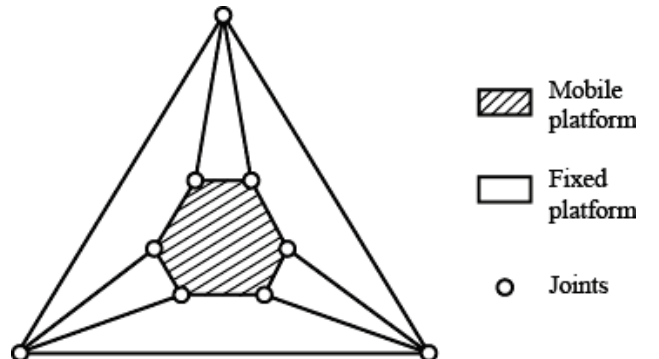


Figure 4. Architecture for the parallel manipulator with binary vertexes in the mobile platform.

Source: The Authors.

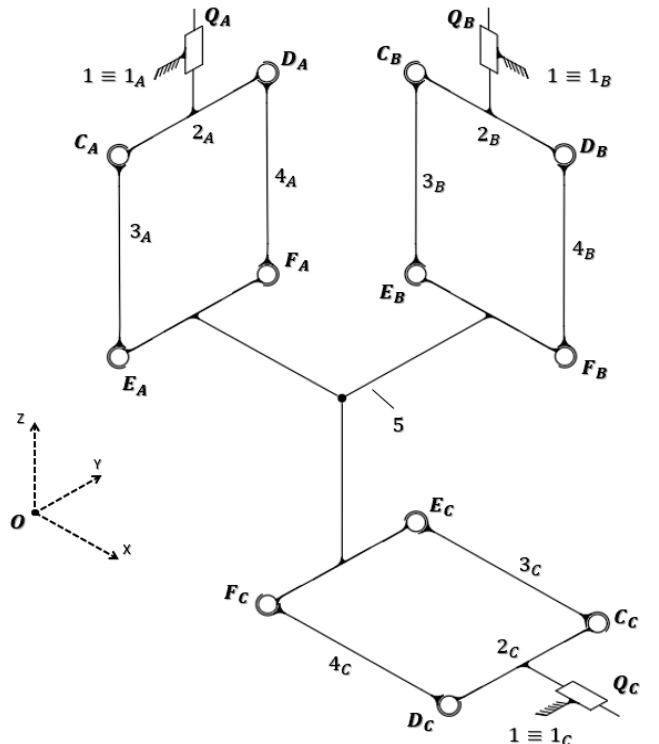


Figure 5. Parallel manipulator's scheme with the architecture  $3\underline{P}Pa^{4S}$ .  
Source: The Authors.

When the morphology of the manipulator was completely defined, the initial position of the manipulator was established (Fig. 6).

The independent variables were defined  $q_1$ ,  $q_2$ , and  $q_3$ , representing the position of the input link with respect to the axis  $Z'$ , which belonged to the fixed reference framework  $(AX'Y'Z')i$ . Subsequently, the manipulator was considered to be in its initial position when the values of the independent variables  $q_1$ ,  $q_2$ , and  $q_3$  were equal to  $q_{i0}$ . Here, the reference framework of the mobile platform ( $PUVW$ ) was located in relation to the reference framework ( $OXYZ$ ) in the position:

$$P_0 = z_0 k \quad (34)$$

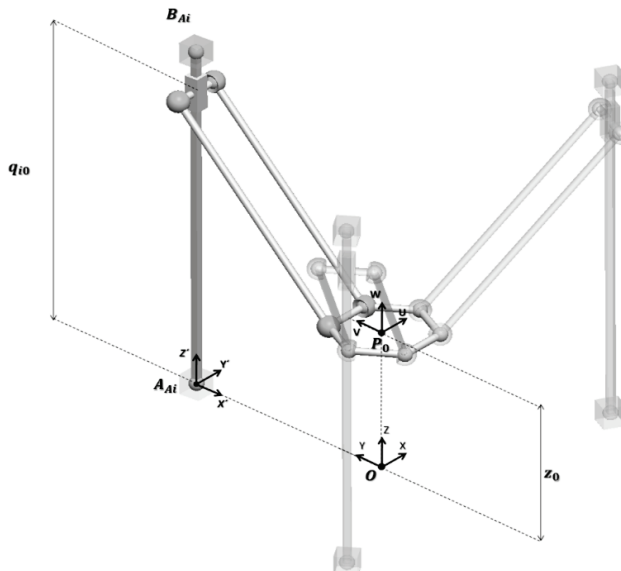


Figure 6. Initial position of the manipulator.  
Source: The Authors.

### 3.3. Dimensional parameters of the manipulator

The dimensional parameters defined in Fig. 3 were calculated by the following preliminary dimensions of the workspace and the maximum and minimum deviation angles:

- Cylinder radius:  $r_0 = 75$  mm,
- Height of the cylinder:  $h = 200$  mm,
- Maximum opening angle:  $\rho = 22.5^\circ$
- Minimum transmission angle:  $\gamma_{\min} = 45^\circ$ ,
- Maximum deviation angle:  $\psi_{\max} = 45^\circ$ ,
- Maximum transmission angle:  $\gamma_{\max} = 77.5^\circ$ ,
- Minimum deviation angle:  $\psi_{\min} = 22.5^\circ$ ,
- Mobile platform Radius:  $r = 40$  mm.

Table 4.  
Dimensional parameters of the manipulator.

Input Data	$h$ [mm]	$r_o$ [mm]	$r$ [mm]	$\psi_{\max}$ [deg]	$\psi_{\min}$ [deg]
	200	75	40	45	22.5
Output Data	$L$ [mm]	$R-r$ [mm]	$R$ [mm]	$Zi_{\min}$ [mm]	$Zi_{\max}$ [mm]
	462.359	251.937	291.937	326.937	627.164

Source: The Authors.

Table 5.  
Calculation process of workspace dimensional parameters.

Input Data	$L$ [mm]	$r$ [mm]	$R$ [mm]	$\psi_{\max}$ [deg]	$\psi_{\min}$ [deg]
	460	40	290	45	22.5
Output Data	$r_o$ [mm]	$R-r$ [mm]	$Zi_{\min}$ [mm]	$Zi_{\max}$ [mm]	$h$ [mm]
	75.27	250	325.27	635.52	210

Source: The Authors.

Considering the previous values and using Eqs. (11)-(14), the consolidated values in Table 4 were obtained:

The resulting values were standardized, and the dimensional parameters of workspace were calculated again, which are shown in Table 5:

After the dimensional parameters of the manipulator were standardized, there were smaller variations in the workspace requested. Therefore, were used as the constructive dimensions of the parallel manipulator.

### 3.3. Stiffness analysis of the manipulator

In this section, we study the behavior of total rigidity in the theoretical and maximum inscribed workspace. Fig. 7 depicts the horizontal cutting planes which were taken with  $z$ -values of 230, 280, 385, and 430 mm.

As Fig. 7 shows, the black areas are those with the lowest values in the total stiffness, while the white ones represent the highest values. The maximum stiffness was adjusted to a value of  $2.5 \times 10^8$  kN/m to obtain a better visualization of the results (although few points reach this value). These areas of increased stiffness coincided with the actuator's arrangement in which the platform reached extreme positions within the maximum inscribed workspace. The lowest value reached was approximately  $10^5$  kN/m; thus, there were no critical points.

### 3.4. Dexterity analysis of the manipulator

Subsequently, the results obtained were analyzed for the condition number in the theoretical and maximum inscribed workspace. Fig. 8 shows the horizontal cutting planes, which were assigned  $z$ -values of 230, 280, 385, and 430 mm.

Figs. 8 and 9 show values of the condition number approximate to one in the central area of the maximum inscribed workspace, presenting values equal to one (isotropic configuration) when the mobile platform was located at  $P_x = 0$  and  $P_y = 0$ .

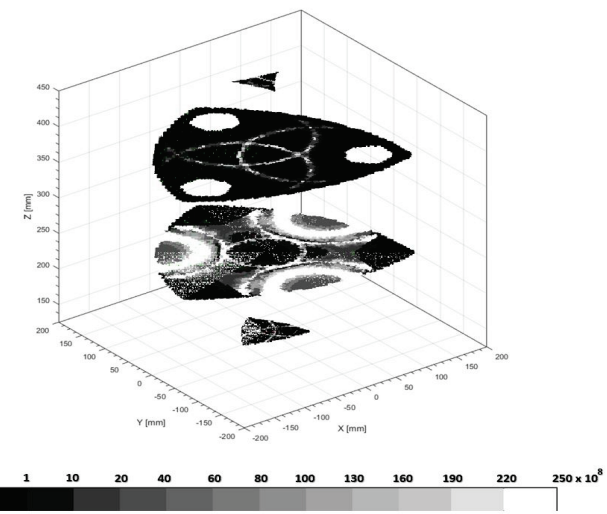


Figure 7. Horizontal cutting planes theoretical workspace (stiffness).  
Source: The Authors.

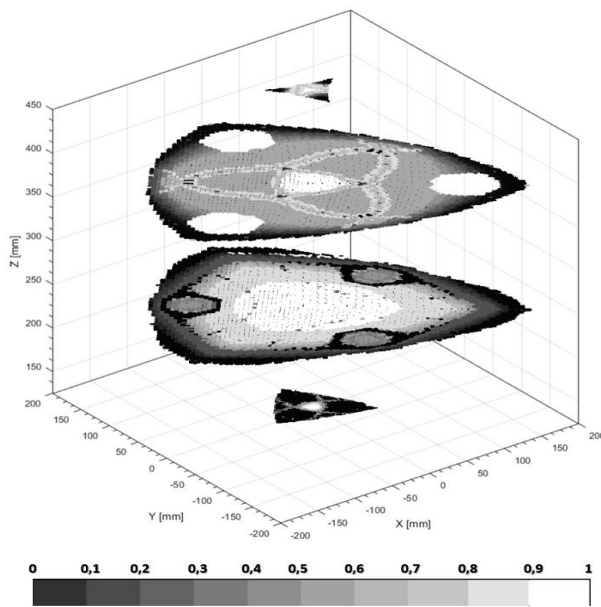


Figure 8. Horizontal planes theoretical workspace (Condition Number).  
Source: The Authors.

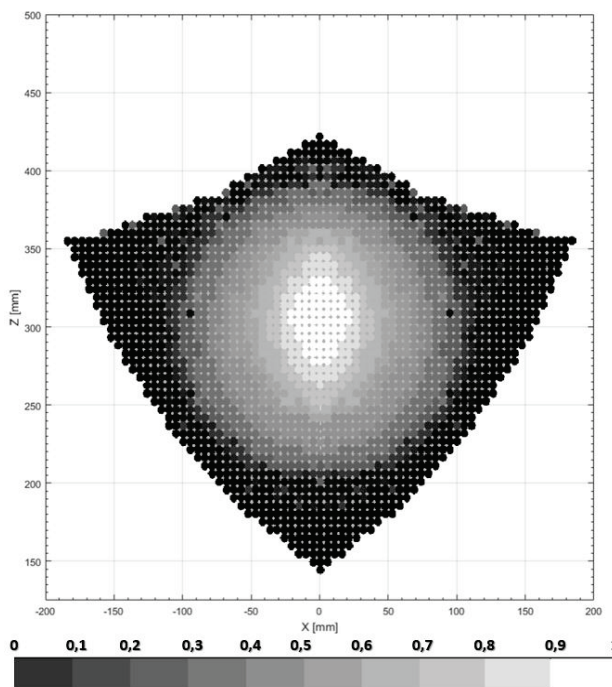


Figure 9. Cutting plane XZ in the maximum inscribed workspace.  
Source: The Authors.

The white area represents high values of the number of conditioning (approximately one), which represents a configuration away from singular positions, while the black area represents the lowest (approximately zero). This zone of conditioning values approximate to one also depended on the position on the z-axis of the mobile platform; within this region, the best behavior of the conditioning number within

the range of values for  $P_z$  between 210 and 420 mm was presented.

Considering the results obtained, the design workspace defined was considered to present values of the condition and stiffness numbers suitable for the operation of the manipulator.

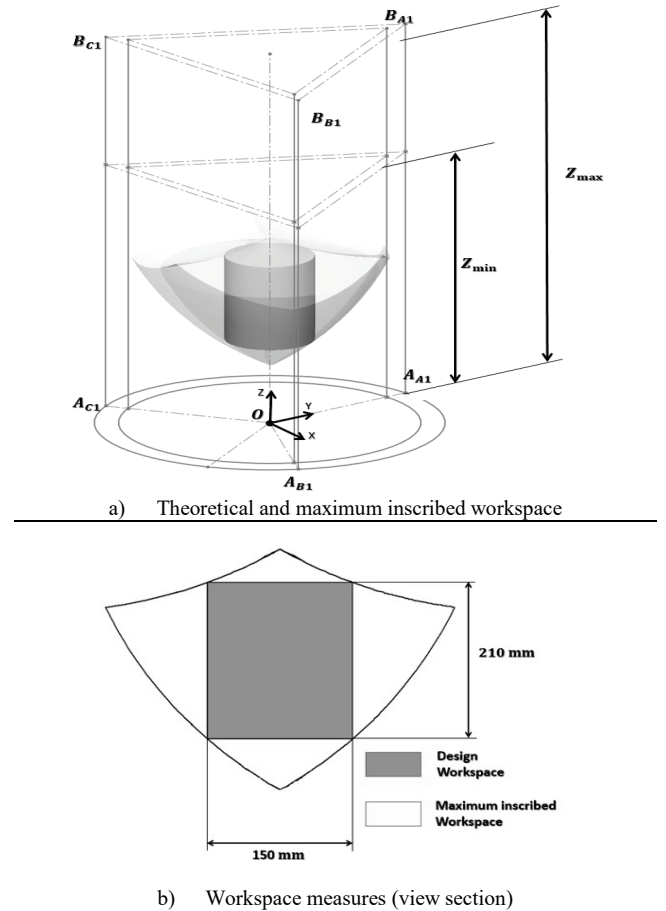


Figure 10. Manipulator's workspace.  
Source: The authors.

Table 6.  
Calculating volume on each workspace for the parallel manipulator

Workspace Name	Morphology	Volume [mm <sup>3</sup> ]
Theoretical		15363236
Maximum inscribed		11122421
Designed		3185626

Source: The Authors.

### 3.5. Manipulator's workspace

CAD was used to obtain the theoretical workspace, enabling the Boolean features with multi-solid bodies to be obtained. Fig. 10 (a) shows the theoretical and maximum registered workspace, in which the workspace design was located, a completely confined cylinder. These can be observed in detail in Fig. 10 (b), where the dimensions of a definite workspace are shown.

Table 6 shows the volumes of every workspace, achieved by the parallel manipulator's design.

## 4. Discussion and conclusions

The proposed methodology for the morphological synthesis enables a significant number of solution alternatives to the kinematic chains to be used in the manipulator to be obtained. From the eleven possible topologies defined, the selection process led us to identify the configuration 3<sub>PPA</sub><sup>4S</sup> as the most promising and viable in terms of the established design criteria. Moreover, the dimensional synthesis, based on the concept of maximum inscribed workspace, enabled the dimensional parameters of the manipulator to be determined and to relate them directly with the proposed dimensions in the design criteria for the workspace. When the dimensional synthesis process was incorporated into the study of the input transmission index, the aim was to generate dimensional parameters in the manipulator which enabled an adequate relation between mobility or force in the manipulator's mobile platform with a low possibility of determining singular positions. The stiffness and dexterity maps were obtained within the manipulator's theoretical workspace in some planes of interest. The results enabled the zones of the best behavior of the condition number to be identified, and no regions of the screen within the manipulator's workspace were observed that do not have utility service due to stiffness. This corroborated the fact that the workspace was designed with the values of the condition number and stiffness suitable for the operation of the manipulator. Finally, the geometrical determination of the manipulator's workspace was conducted using computer-aided design to obtain the theoretical maximum inscribed workspace. The result of the study is useful for the design and application of parallel manipulators, as it addresses the process of morphological synthesis and dimensional process in a more practical manner. The methods used in this study can be applied to design other parallel manipulator configurations, in which linear actuators are included as input elements.

## References

- [1] Zhang, D., Parallel robotic machine tools. Springer, New York, USA, 2010.
- [2] Lou, Y., Liu, G., Xu, J. and Li, Z., A general approach for optimal kinematic design of parallel manipulators. IEEE International Conference on Robotics and Automation, IEEE, New Orleans, LA, USA, pp. 3659-3664, 2014. DOI: 10.1017/S0263574719001577
- [3] Hesse, S., Modular pick-and-place devices. From the series Blue Digest on Automation. FESTO AG & Co, Esslingen, Germany, 2000.
- [4] Tam, T., Open Beam, [online]. Redmond, WA. [cited: July 10<sup>th</sup> of 2017]. Available at: URL:<http://www.openbeamusa.com/>.
- [5] Wygant, S., SeeMeCNC Team Stefan, [online]. Ligonier, Indiana, USA. [cited: July 10<sup>th</sup> of 2017]. Available at: URL:<https://www.seemecnc.com/>
- [6] Dinga, H., Fenga, Z., Yang, W. and Kecskeméthy, A., Structure synthesis of 6-DOF forging manipulators, Mechanism and Machine Theory, 111, pp. 135-151, 2017. DOI: 10.1016/j.mechmachtheory.2017.01.001
- [7] Kong, X. and Gosselin, C., Type synthesis of 3-DOF Translational parallel manipulators based on screw theory, ASME Journal of Mechanical Design, 126 pp. 83-92, 2004. DOI: 10.1115/1.1637662
- [8] Lee, C.C. and Hervé, J.M., On the enumeration of schoenflies motion generators, Proceedings of The 9<sup>th</sup> IFToMM International Symposium on Theory of Machines and Mechanisms, Bucharest, Romania, 2005.
- [9] Rezaei, A. and Akbarzadeh, A., Study on Jacobian, singularity and kinematics sensitivity of the FUM 3-PSP parallel manipulator, Mechanism and Machine Theory 86, pp. 211-234, 2015. DOI: 10.1016/j.mechmachtheory.2014.11.009
- [10] Meng, J., Liu, G. and Li, Z., A Geometric theory for analysis and synthesis of Sub-6 DOF parallel manipulators. IEEE Transactions on Robotics and Automation 24, pp. 625-649, 2007. DOI: 10.1109/TRO.2007.898995
- [11] Gogu, G., Structural synthesis of fully-isotropic translational parallel robots via theory of linear transformations, European Journal of Mechanics A/Solids 23, pp. 1021-1039, 2004. DOI: 10.1016/j.euromechsol.2004.08.006
- [12] Goldsztajna, A., Caro, S. and Chabert, G., A three-step methodology for dimensional tolerance synthesis of parallel manipulators, Mechanism and Machine Theory, pp. 213-234. 2016. DOI: 10.1016/j.mechmachtheory.2016.06.013
- [13] Gogu, G., Fully-isotropic parallel manipulators with five degrees of freedom, IEEE International Conference on Robotics and Automation, Orlando, Florida, USA, 2006, pp. 1141-1146. DOI: 10.1109/ROBOT.2006.1641864
- [14] Dolga, V. and Dolga, L., The structural synthesis of the parallel robots. Mechanika 17, pp. 288-295, 2011. DOI: 10.5755/j01.mech.17.3.505
- [15] Tsai, L.W., Robot analysis: the mechanics of serial and parallel manipulators. Wiley, New York, USA, 1999.
- [16] Liu, X.J. and Wang, J., Parallel kinematics: type, kinematics, and optimal design. Springer, New York, USA, 2014.
- [17] Liu, X.J., Wang, J. and Oh, K.K., A New approach to the design of a DELTA robot with a desired workspace. Journal of Intelligent and Robotic Systems, pp. 209, 2004. DOI: 10.1023/B:JINT.0000015403.67717.68
- [18] Tao, D.C., Applied linkage synthesis. Addison-Wesley, Reading, 1964, pp. 7-12.
- [19] Sharma, C.S. and Purohit, K., Theory of mechanisms and machines. Eastern Economy eds. Prentice-Hall, New Delhi, India, 2006.
- [20] Martin, G.H., Kinematics and dynamics of machines. McGraw-Hill, New York, USA, 1982.
- [21] Gao, Z., Zhang, D., Hu, X. and Ge, Y., Design, analysis and stiffness optimization of a three degree of freedom parallel manipulator, Robotica, 28, pp. 349-357, 2010. DOI: 10.1017/S0263574709005657
- [22] Kelaiaina, R., Company, O. and Zaatri, A., Multiobjective optimization of a linear Delta parallel robot, Mech. Mach. Theory, 50, pp. 159-178, 2012. DOI: 10.1016/j.mechmachtheory.2011.11.004
- [23] Liu, X.J., Wang, J. and Gao, F., Performance atlases of the workspace for planar 3-DOF parallel manipulators. Robotica, 18, pp. 563-568, 2000. DOI: 10.1017/S0263574700002678
- [24] Liu, X.J., Wang, J. and Zeng, H., Workspace atlases for the computer - aided design of the Delta Robot. Journal of Mechanical Engineering Science, 217, pp. 861-869, 2003. DOI: 10.1243/095440603322310413
- [25] Arsenault, M. and Boudreau, R., Synthesis of planar parallel mechanisms while considering workspace, dexterity, stiffness and singularity avoidance, Journal of Mechanical Design, 128, pp. 69, 2006. DOI: 10.1115/1.2121747
- [26] Cao, W., Yang, D. and Ding, H., A method for stiffness analysis of overconstrained parallel robotic mechanisms with Scara motion,

- Robotics and Computer-Integrated Manufacturing 128, pp. 426-435, 2018. DOI: 10.1016/j.rcim.2017.08.014
- [27] Gabardi, M., Solazzi, M. and Frisoli, A., An optimization procedure based on kinematics analysis for the design parameters of a 4-UPU parallel manipulator, Mechanisms and Machine Theory 133, pp. 211-228, 2019. DOI: 10.1016/j.mechmachtheory.2018.11.015
- [28] Raoofian, A., Taghvaeipour, A. and Kamali A., On the stiffness analysis of robotic manipulators and calculation of stiffness indices, Mechanism and Machine Theory, 130, pp. 382-402, 2018. DOI: 10.1016/j.mechmachtheory.2018.08.025
- [29] Itul, T., Gherman, B. and Pîsla, D., Comparative study of Two 2-DOF parallel mechanisms used for orientation, Mechanisms and Machine Science, 18, pp 145-157, 2014. DOI: 10.1007/978-3-319-01845-4\_15
- [30] Liu, X.J., Jin, Z.L. and Gao, F., Optimum design of 3-DOF spherical parallel manipulators with respect to the conditioning and stiffness indices, Mechanism and Machine Theory 35, pp. 1257-1267, 2000. DOI: 10.1016/S0094-114X(99)00072-5
- [31] Pashkevich, A., Chablat, D. and Wenger, P., Stiffness analysis of overconstrained parallel manipulators. Mechanism and Machine Theory 44, pp. 966-982, 2009. DOI: 10.1016/j.mechmachtheory.2008.05.017
- [32] Quintero, H.F., Mejia, L.A., Holguin, G., Diaz M.A., Herrera M, Mesa, C.A. and Daravilla, D., Manipuladores paralelos, síntesis, análisis y aplicaciones, Universidad Tecnológica de Pereira, Pereira, Colombia, 2018, pp. 137-146.
- [33] Quintero, H.F., Mejia, L.A. and Diaz, M.A., Synthesis of planar parallel manipulators including dexterity, force transmission and stiffness index, Mechanics Based Design of Structures and Machines, 2019. DOI: 10.1080/15397734.2019.1615503

**C.A. Mesa-Montoya**, received a BSc. Eng. Mechanical Engineering in 2008 and MSc. in Mechanical Engineering in 2017. He is currently an Assistant professor and since 2015, he has worked for the Universidad Tecnológica de Pereira, Colombia in the publication of scientific papers and peer-review conference-proceedings papers. His current research interests include mechanical design, modeling, co-simulating, and development for parallel mechanism oriented toward upper and lower limb assistance and rehabilitation.

ORCID: 0000-0002-9353-4575.

**H.F. Quintero-Riaza**, received a BSc. Eng Mechanical Engineering in 1994, MSc. in Mechanical Engineering in 2000, and PhD in Mechanical Engineering in 2006. Since 1997, he has worked for the Universidad Tecnológica de Pereira, Colombia in the publication of scientific journals and as a professor for the Mechanical Engineering Department. He is also currently the director of the Research group of Manufacture Processes and Machines Design and the coordinator of the Mechanic Vibration Laboratory of the university.

ORCID: 0000-0002-4275-739X.

**F. Gutiérrez-Madrid**, received a BSc. Eng Mechanical Engineering in 2018. He is an active member of the Research group of Manufacture Processes and Machines Design of the Universidad Tecnológica de Pereira, Colombia. Currently, he works for the Universidad Tecnológica de Pereira in the publication of scientific journals, researching and as a professor for the Mechanical Engineering Department.

ORCID: 0000-0002-1477-8994



UNIVERSIDAD NACIONAL DE COLOMBIA

SEDE MEDELLÍN  
FACULTAD DE MINAS

## Área Curricular de Ingeniería Mecánica

### Oferta de Posgrados

Doctorado en Ingeniería - Mecánica y  
Mecatrónica

Maestría en Ingeniería - Ingeniería  
Mecánica

Especialización en Mantenimiento

Mayor información:

E-mail: acmecanica\_med@unal.edu.co  
Teléfono: (57-4) 4259262